Available online at www.sciencedirect.com

SciVerse ScienceDirect

Ceramics International 38 (2012) 2051–2058

CERAMICS INTERNATIONAL

www.elsevier.com/locate/ceramint

Effect of atomization methods on the size and morphology of $Gd_{0.1}Ce_{0.9}O_{2-\delta}$ powder synthesized by aerosol flame synthesis

Jongmo Im [a,b], Inyu Park [c], Dongwook Shin [b,c,*]

[a] Industrial Technology Support, Korea Institute of Materials Science, Changwon 642-831, Republic of Korea
[b] Division of Materials Science & Engineering, Hanyang University, Seoul 133-791, Republic of Korea
[c] Department of Fuel Cells and Hydrogen Technology, Hanyang University, Seoul 133-791, Republic of Korea

Received 25 July 2011; received in revised form 18 October 2011; accepted 18 October 2011
Available online 23 October 2011

Abstract

Nano-sized gadolinium doped ceria (GDC) powders were successfully synthesized by aerosol flame deposition (AFD) with two different atomization methods; ultrasonic and electrostatic atomization. The effect of the atomization method on the size and morphology of GDC particles were investigated. It was observed that the diameter range of the GDC small primary particles synthesized by the ultrasonic atomization method was 10–50 nm while with the electrostatic method was 5–25 nm. In addition, the size of primary large particle found to be decreased from 200 nm to 50 nm with increasing electric field up to 15 kV. The GDC powder synthesized by the electrostatic atomization exhibited reduced crystallite size, particle size, and similar electrical conductivity compared to GDC powder synthesized by ultrasonic atomization. This work demonstrated the benefits of the electrostatic atomization for producing smaller-sized GDC nanopowders for the application in intermediate temperature solid oxide fuel cells.

Keywords: Gadolinium doped ceria (GDC); Aerosol flame deposition (AFD); Ultrasonic atomization; Electrostatic atomization; Solid oxide fuel cells (SOFCs); Nanopowders

1. Introduction

Solid oxide fuel cells (SOFCs) have received special interests due to their several advantages such as the high efficiency in energy conversion, low pollution emission, and highly flexible operation with various fuels [1]. However, the high operating temperature of 800–1000 °C is a main disadvantage due to safety and maintenance issues. In order to reduce the operating temperature and increase the ionic conductivity, various approaches are applied to lower the resistance of dense electrolyte membranes: decreasing electrolyte thickness or using alternative materials with higher ionic conductivity at lower temperature [2]. Furthermore, it is reported that nanosized cerium oxide (CeO_2) showed extra ordinary enhanced electrical properties than microcrystalline specimens [3,4]. With higher ionic conductivity at relatively moderate temperature (above 600 °C), doped ceria has been extensively studied as an electrolyte [3,4]. Among various kinds of doped ceria, gadolinium-doped ceria (GDC) has been considered to be one of the most promising electrolytes for intermediate temperature SOFCs(IT-SOFCs) operated below 800 °C. The ionic conductivity of ceria-based electrolyte is primarily related to the dopant, composition, microstructure, impurity and fabrication processes [5].

Traditional preparation methods of ceria-based particles include co-precipitation [6], hydrothermal synthesis [7], sol–gel [8]. Unlike these nanosized oxide powder techniques, the advantages of aerosol flame deposition (AFD) process are a wide choice of nonvolatile precursors including liquid precursors, high degree of crystallinity of as-prepared metal oxide nanoparticles, and the capability to produce virtually any kind of oxide nano-sized powders that can be synthesized by solid state reactions. However, the control of particle size, morphology, crystalline phase, and composition are difficult due to the harsh environment such as steep temperature gradients and rapid particle evolution. To control the aerosol

* Corresponding author. Tel.: +82 2 2220 0503; fax: +82 2 2220 4011.
E-mail address: dwshin@hanyang.ac.kr (D. Shin).

0272-8842/$36.00
doi:10.1016/j.ceramint.2011.10.041

reaction in flame reactors, precise information about nano-sized particle generation in terms of size distribution, shape, composition and phase is needed [9–12]. Critical factors for control in the AFD process are the size and uniformity of the feed aerosol droplets. There are various atomizers which can be categorized according to the type of energy used for atomization. Among the types of atomizers, ultrasonic and electrostatic atomizers are commonly used to produce aerosol droplets [13].

In this paper, the size and morphology of synthesized particles as well as flame temperature were investigated at local positions in co-flow diffusion flames. In particular, we focus on the effects of two different atomizers and electric field on the size and morphology of synthesized particles.

2. Experimental procedure

2.1. Synthesis of the GDC powder by AFD

The configuration of AFD apparatus was described in detail in the previous paper [14]. Briefly, the AFD instrument consists of precursor solution supply zone, droplet atomization zone and flame hydrolysis reaction zone. Both ultrasonic and electrostatic atomizers were used for generating droplets in this work.

The ultrasonic atomizer includes a 1.7 MHz resonator producing short wavelength to disperse a liquid precursor solution into micro-sized droplets. The electrostatic atomizer includes an external-mixing air-assisted nozzle, which is made of two concentric stainless-steel tubes (NanoNC, Korea) as shown in Fig. 1. The outer tube has an outer diameter of 0.71 mm and the inner tube has an outer diameter of 0.31 mm. The external-mixing air-assisted nozzle breaks precursor solution into small droplets by means of a stream of argon gas (1 slm/min) at high velocity. Simultaneously, the nozzle is charged with an electric field by high DC voltage power supply (voltage range ~20 kV), where the electric field induced force due to the surface charge density exceeds the surface tension resulting in the droplet breaking up into finer droplets. The atomized droplets were carried by Ar carrier gas into a flame hydrolysis reaction zone in an oxy-hydrogen torch. The essential part of the system is the oxy-hydrogen torch, which is made from four concentric tubes creating three concentric gaps, and one shield tube keeping flame stable. Precursor solution flows through the centermost tube of the torch while hydrogen, argon and oxygen flow through three gaps having different width to ensure laminar flow of gases.

The transverse oxy-hydrogen flame temperature of AFD was measured by an R-type thermocouple. Fig. 2 shows transverse temperature distribution of oxy-hydrogen co-flow diffusion flame along the axial direction at various positions (d = 2, 3.5, and 5 cm). In Fig. 2, d and t represent the axial distance away from the torch and the transverse distance from the center, respectively. The luminous part of the flame extended down to d = 8 cm at which the flame temperature was not measured because the flame flow was unstable due to the suction by the exhaust system. The maximum flame temperature was measured to be 1698 K at the location of d = 2 cm and t = 3 mm. The temperature of the upper flame is higher than the lower flame due to thermal convection. The high flame temperature is believed to enable the formation of the plasma supersaturated with reactive gaseous phases.

For preparing precursor solutions, cerium nitrate hexahydrate, $Ce(NO_3)_3{\cdot}6H_2O$ [Aldrich, >99.9%] and gadolinium nitrate hexahydrate, $Gd(NO_3)_3{\cdot}6H_2O$ [Aldrich, >99.9%] were used as precursors and then ultrasonically agitated in methanol

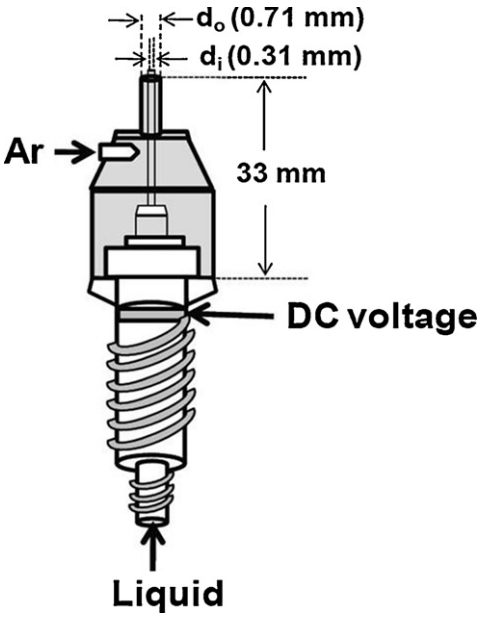

Fig. 1. A schematic diagram of an external-mixing air-assisted nozzle for electrostatic atomization.

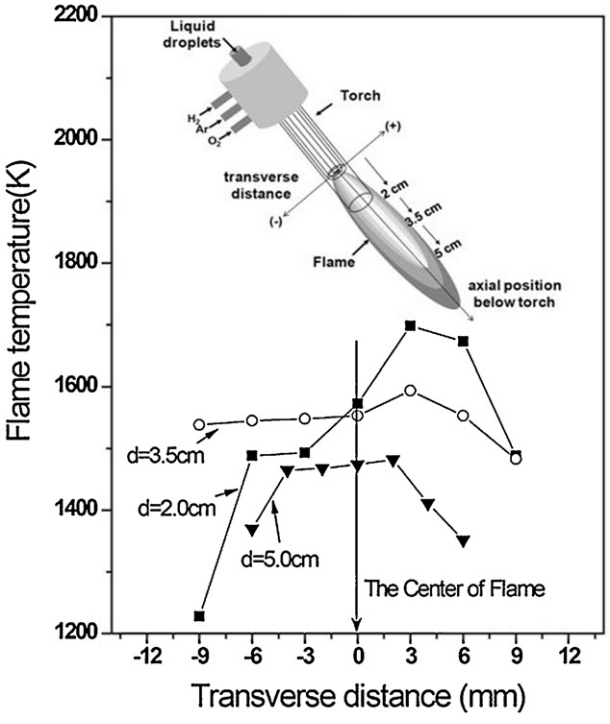

Fig. 2. Transverse temperature distribution of oxy-hydrogen co-flow diffusion flame along the axial direction at various positions (d = 2, 3.5, and 5 cm).

[CARLO ERBA, >95.0%] at room temperature to obtain a 0.05M Gd:Ce = 0.1:0.9 solution. $Gd_{0.1}Ce_{0.9}O_{2-x}$ powders were synthesized with a pre-determined optimum process condition such as precursor solution concentration of 0.05 M, hydrogen flow rate of 3.0 l min^{-1}, oxygen flow rate of 7.5 l min^{-1}, and argon flow rate 1.0 l min^{-1}. The GDC powders synthesized by AFD with ultrasonic and electrostatic atomization were designated as GDC_{UP} and GDC_{EP}, respectively.

2.2. Characterization of the GDC powder

For investigating the phase and crystallinity of the as-prepared GDC powders, the X-ray diffraction pattern was measured by a Rigaku ULTIMA IV diffractormeter. Data were collected in Bragg–Brentano geometry CuKα radiation with a step size of 0.05° in a 2θ range of 20° to 90°. The crystallite size of the as-prepared GDC particle was calculated from full width at half maximum (FWHM) using the Scherrer's formula. The particle diameter is given by

$$D = \frac{0.9\lambda}{\beta \ \mathrm{Cos} \ \theta} \tag{1}$$

where D is the crystallite size in nm, λ the radiation wavelength (0.154056 nm in present case, Cu target), θ the diffraction angle, and β is the corrected line width at half peak intensity, β can be calculated using the formula:

$$\beta^2 = \beta_m^2 - \beta_s^2 \tag{2}$$

where β_m is the measured FWHM and β_s is the FWHM of a standard silicon sample (0.1704) [15].

The morphology and size of the as-prepared GDC particles were characterized in plan-view using a scanning electron microscope (NOVA, NANO 200) and transmission electron microscope (JEOL, JEM-3010). The diameter of particles was measured from SEM and TEM images and the mass distribution $m(D)$ of the particle size was calculated from the number-to-mass conversion [16]. The mass distribution is given by

$$m(D) = \left(\frac{\pi}{6}\right) \cdot D^3 \cdot \rho \cdot n(D) \tag{3}$$

where D is the diameter of the particles in nm, ρ is the material density, and $n(D)$ is the number of the particles.

2.3. Electrical characterization

The GDC powders were used to prepare the cylindrical pellet-form specimens (0.8 cm in diameter, 0.7 mm in

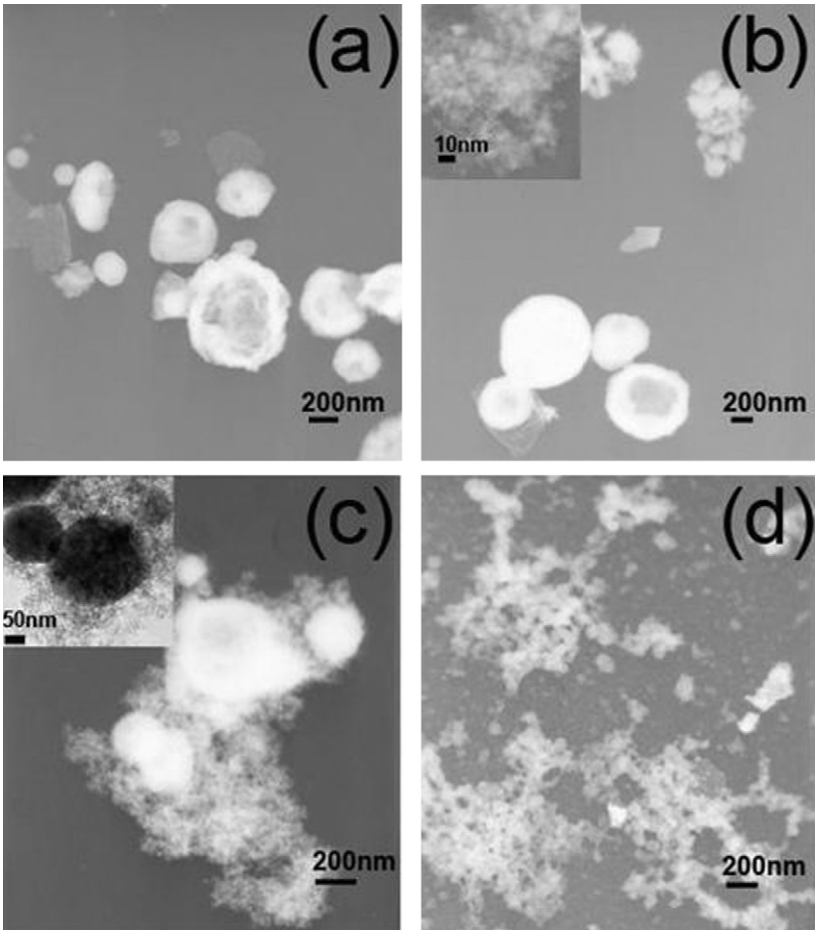

Fig. 3. TEM images of the GDC_{EP} synthesized at optimal process conditions and collected by thermophoretic sampling at various axial positions below the torch in oxy-hydrogen co-flow flame. (a) X = 2 cm, (b) X = 3.5 cm, (c) X = 5 cm, and (d) X = 8 cm.

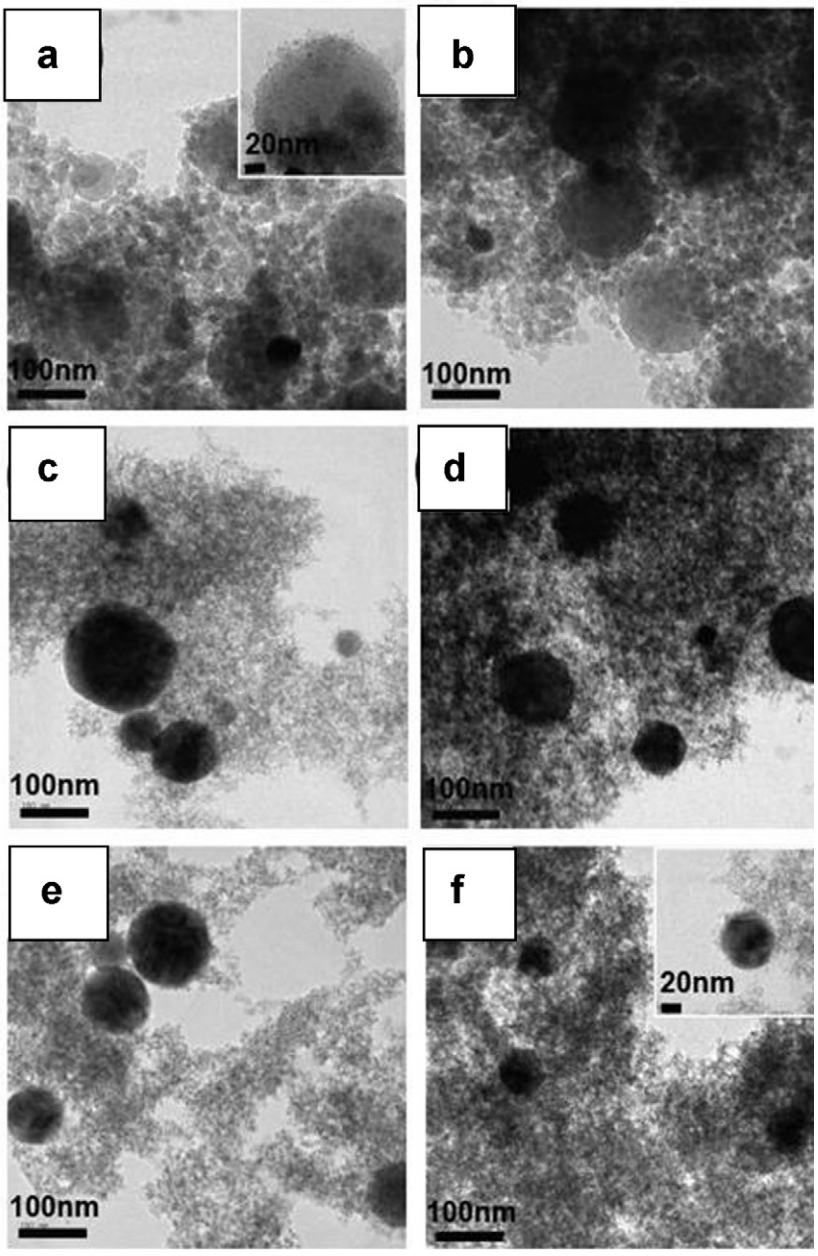

Fig. 4. TEM images of the GDC_{EP} synthesized as a function of DC voltages. (a) 0 kV, (b) 3 kV, (c) 6 kV, (d) 9 kV, (e) 12 kV, and (f) 15 kV.

thickness) was obtained by dry pressing at 20 MPa and was sintered at 1350 °C for 2 h in an electric furnace. The real density of the pellet was measured by Archimedes method and reaches ~90% of theoretical density. The GDC pellets prepared with GDC powders synthesized by AFD with ultrasonic and electrostatic atomization were designated as GDC_{UP} and GDC_{EP}, respectively. The SEM images were analyzed to estimate the average grain size by linear intercept method. The average grain size of the GDC_{UP} was 2.8 μm, while that of the GDC_{EP} was 0.9 μm (see inset of Fig. 9). The Pt paste (Nilaco, Japan) was painted on both the flat sides of the sintered samples and heated to 700 °C. Electrical measurements were carried out with Solartron electrochemical system consisting of the SI 1287 electrochemical interface and the 1260 frequency response analyzer. AC impedance was measured between 550 and 750 °C with increment of 50 °C. For AC impedance measurements, 20 mV, AC signal (frequency from 10^{-3} to 10^{6} Hz) was applied to the samples. The experimental data of AC impedance were collected and analyzed by the commercial software packages Zplot/Zview to separate the contribution of bulk, grain boundary, and electrolyte–electrode interface.

3. Results and discussion

3.1. Nanopowder prepared with the electrostatic atomizer

The optimal process conditions for synthesizing GDC particles using droplets generated by the ultrasonic nebulizer were investigated in the previous work [17]. For comparison, the growth of GDC particles and the effect of DC voltage on the

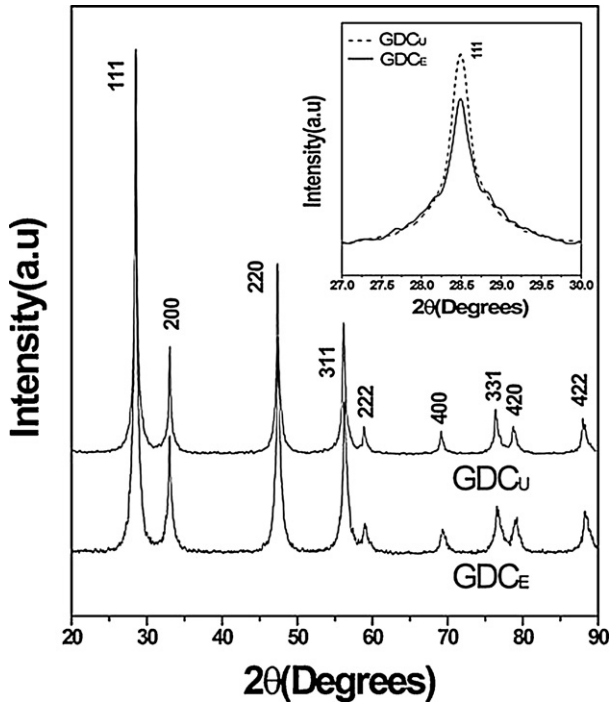

Fig. 5. XRD patterns of the GDC_{UP} and GDC_{EP} and the peaks indexed to the cubic structure of ceria. (Insert) detailed peak shape showing the FWHM of the (1 1 1) peak.

morphology of GDC particles, prepared by an electrostatic atomizer, were studied in this work. Fig. 3 shows TEM images of GDC particles, synthesized from droplets generated by the electrostatic atomization without an applied positive voltage, collected by thermophoretic sampling on a molybdenum TEM grid at four axial positions of 2, 3.5, 5, and 8 cm below the torch. At the flame axis $X = 2$ cm, several hundred nanometer (∼700 nm) single primary particles were observed [Fig. 3(a)]. At this position, the short residence time in the flame results in the formation of large and spherical single primary particles due to incomplete evaporation of the liquid solvent and incomplete pyrolysis of the dissolved precursors. At the flame axis $X = 3.5$ cm, we observed not only the large, dense, spherical, unagglomerated particles, but also particles with smaller diameter and loose agglomeration [Fig. 3(b)]. At $X = 3.5$ cm, the flame temperature is lower and the particle residence time is longer, which promotes gas phase precipitation of the supersaturated solute vapor in the plasma gas forming small primary nanoparticles. At the flame axis $X = 5$ cm, hard agglomerates composed of both the large and small particle size were observed as shown in Fig. 3(c). At this position, the flame temperature is low enough to increase the degree of supersaturation of the solute vapor in the plasma gas, resulting in smaller (10–20 nm) primary particles. The agglomerate appears to be sintered into more dense and hard aggregates. Finally, at flame axis $X = 8$ cm (nearby the intake of exhaust system), longer particle residence time and low flame

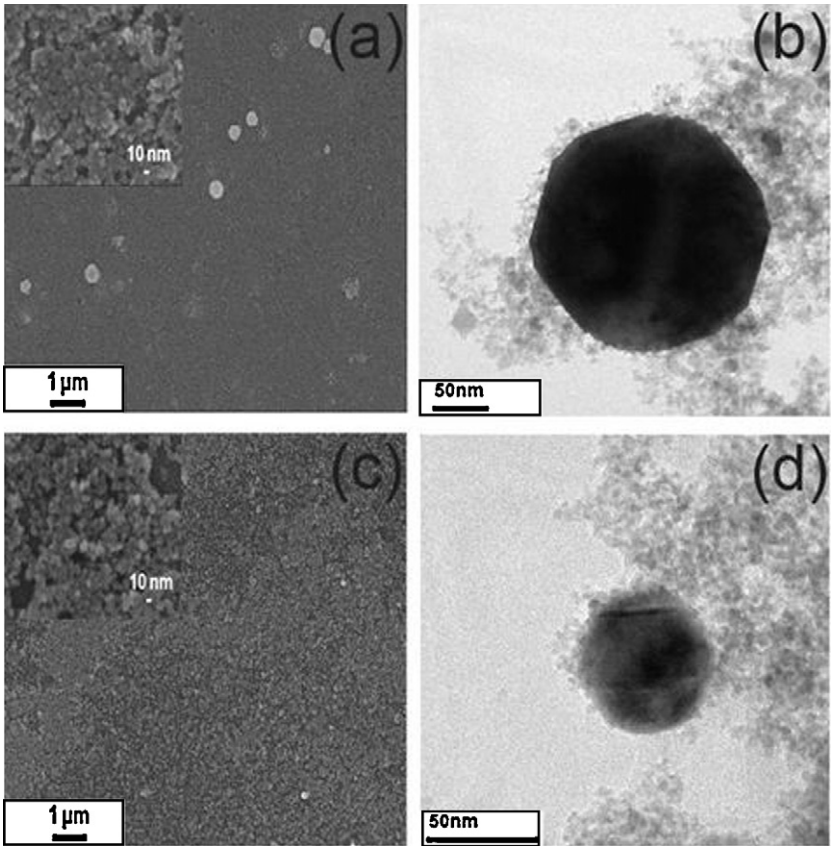

Fig. 6. The comparison of the SEM and TEM images between the GDC_{UP} and GDC_{EP}. (a), (b) for GDC_{UP}, (c) and (d) for GDC_{EP}.

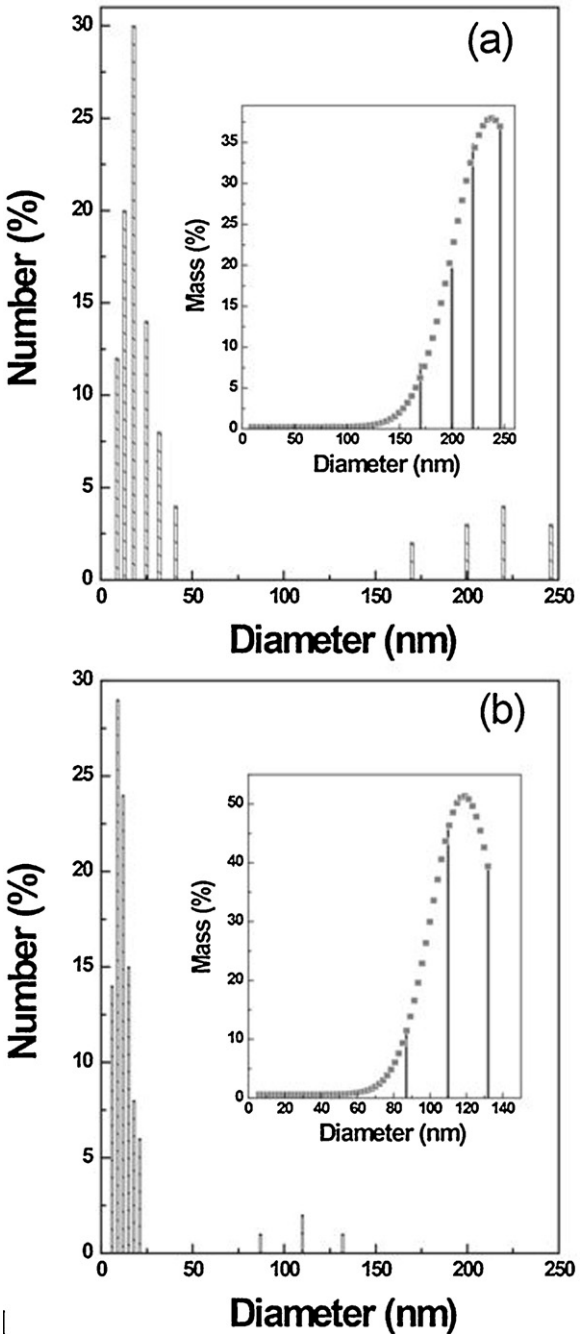

Fig. 7. Particle size and mass distribution (insert) of (a) the GDC_{UP} and (b) GDC_{EP}.

temperature causes even a higher degree of agglomeration of small single primary particles due to the Brownian coagulation and sintering.

From above observations, it is clear that the mechanisms of particle formation can be classified into two distinct categories; (i) the direct pyrolysis of the liquid droplets at short distances from the torch tip; large particles are formed by the rapid evaporation of liquid solvent at high temperature and condensation and precipitation of dissolved precursors and (ii) gas phase nucleation and growth within the plasma gas and subsequent coagulation; small particles are formed by the plasma reaction. The precursor solution is evaporated completely and dissociated into ions in the flame and formed into gaseous thermal plasma. The plasma gases will be supersaturated at the region of lower temperature, and experience the gaseous nucleation and growth process [18].

Fig. 4 shows the TEM images of GDC particles synthesized from precursor droplets discharged by the electrostatic atomization method as a function of the applied positive voltage. The size of the large primary particle mode decreased from 100–200 nm to 50–150 nm with increasing positive voltage from 0 to 15 kV. The decrease in particle size is attributed to the decrease in the size of generated droplets. As the voltage is increased, the force due to the surface charge

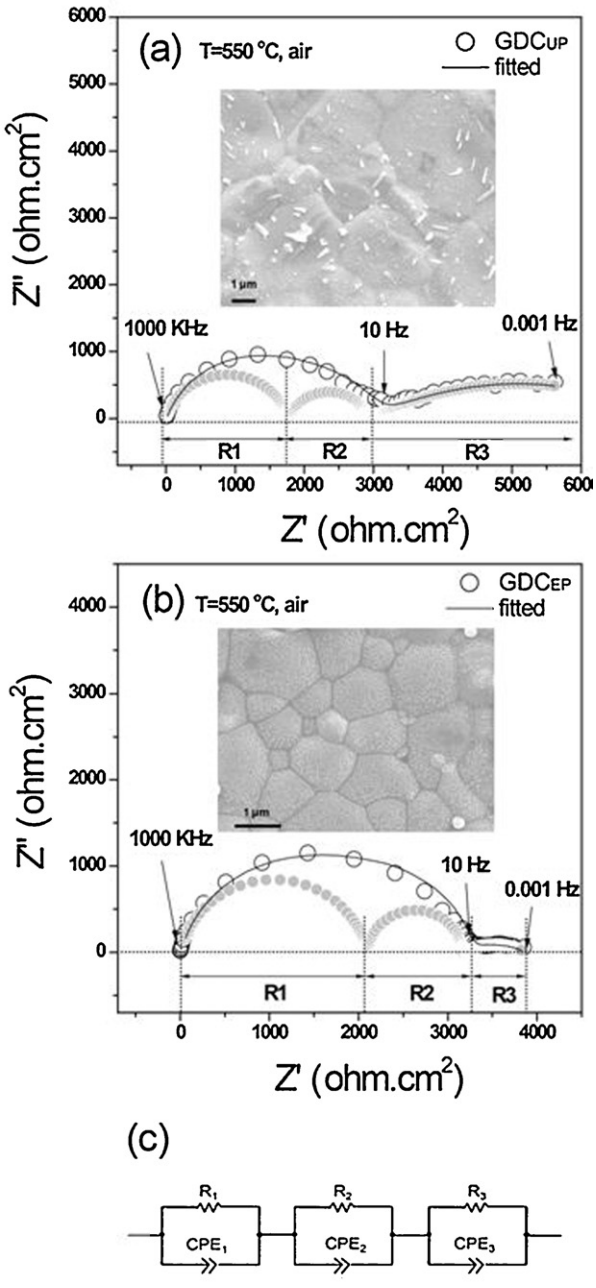

Fig. 8. The AC impedance plots and equivalent circuit (c) of (a) the sintered GDC_{UP} and (b) GDC_{EP} measured at 555 °C in air.

density increases and results in the droplet breaking up into finer droplets [19].

3.2. Morphology and size

The XRD patterns of GDC_{UP} and GDC_{EP} as shown in Fig. 5, exhibited the diffraction peaks of ceria with fully crystallized cubic structure. The crystallite sizes of the GDC particles were calculated from the full width at half maximum (FWHM) using Scherrer's formula, for the (1 1 1) crystal plane of $Gd_{0.1}Ce_{0.9}O_{2-x}$ [inset Fig. 5]. The crystallite sizes of the GDC_{UP} were 14.6 nm and 8.3 nm for the GDC_{EP}.

Fig. 6 shows SEM and TEM images of GDC particles generated using two different atomization methods. The effects of atomization method on the diameter range and the mass distribution $m(D)$ of the particle size was calculated from the number-to-mass conversion as shown in Fig. 7. From the SEM and TEM micrographs, one can see that the size and number of large particles for GDC_{EP} decreased compared with those of GDC_{UP}. It is observed from Fig. 7 that the GDC_{UP} consists of large particles with diameter of 150–250 nm and small particles with diameter of 10–50 nm while GDC_{EP} consists of the particles with reduced sizes; large particles of 50–150 nm and small particles of 5–25 nm. In addition, 96% of the GDC_{EP} were less than 25 nm while 76% of the GDC_{UP} were less than 25 nm. The fraction by the mass of large particle population of 150–250 nm for GDC_{UP} is from 8 to 99% while the fraction by the mass of large one of 50–150 nm for GDC_{EP} is from 11 to 96%. The size of the particle is strongly dependent on the droplet size generated by the atomizer [20]. It was reported that the size range of droplet generated by ultrasonic and electrostatic atomizer are 1–100 μm [21] and 0.04–2 μm [22], respectively. Therefore, the size reduction of the large particle (pyrolysis mechanism) for the GDC_{EP} compared to that of the GDC_{UP} is ascribed to the smaller size of droplets generated by the electrostatic atomization.

It is not clear yet why the size of small particle, synthesized in gas phase, also slightly decreased. One possible explanation is the reduced evaporation enthalpy of the charged droplets generated by the electrostatic atomizer and, thus, the increased degree of supersaturation in plasma gas phase. As a result, the high supersaturation enhances the nucleation rate and decreases primary particle size.

3.3. Electrical property

Fig. 8(a) and (b) show the typical impedance spectra of GDC_{UP} and GDC_{EP} measured at 550 °C in air. There are two depressed semicircles indicating three different contributions due to bulk, grain boundary and electrode–electrolyte interface from high frequency (1000 kHz) to low frequency (0.001 Hz). In order to separate the contributions of two semicircles, an equivalent circuit, $(R_1CPE_1)(R_2CPE_2)(R_3CPE_3)$, is used to fit the data as shown in Fig. 8(c). The fitting results are also summarized in Table 1, which illuminated as lines in Fig. 8(a) and (b). The resistance R_1, R_2 and R_3 stands for the resistance related to bulk, grain boundary, and electrode–electrolyte interface, respectively. CPE is a simple distributed element which produces impedance having a constant phase angle in complex plane. T and P are two parameters in the mathematic expression of the impedance of CPE components shown below,

Table 1
Fitting results of the GDC_{UP} and GDC_{EP} at 550 °C in air.

	GDCUP	GDCEP
R_1 (Ω)	1765	2100
CPE_1-T	9.9×10^{-8}	9.1×101^{-9}
CPE_1-P	0.82	0.86
C_1 (F cm^2)	1.2×10^{-11}	4.2×10^{-12}
R_2 (Ω)	1180	1070
CPE_2-T	1.2×10^{-6}	2.8×10^{-8}
CPE_2-P	0.75	0.94
C_2 (F cm^2)	1.5×10^{-10}	3.1×10^{-9}
R_3 (Q)	4300	700
CPE_3-T	6.7×10^{-5}	5.2×10^{-4}
CPE_3-P	0.3	0.3
C_3 (F cm^2)	3.6×10^{-8}	4.9×10^{-5}

$$Z(\mathrm{CPE}) = \frac{1}{T(\omega i)^P} \tag{4}$$

The exponent P determines this angle. In the special case of $P = 1$, the CPE acts like a capacitor with T equal to the capacitance. The CPE can also yield an inductance when $P = -1$, or a resistance when $P = 0$. The fitting parameters for the spectra are the resistance R, P, and T, which is related to the angular relaxation frequency ω and capacitance C, as follows,

$$\omega = \left(\frac{T}{C}\right)^{1/1-P} = \frac{1}{RC} \tag{5}$$

and thus:

$$C = R^{1-P/P}T^{1/P} \tag{6}$$

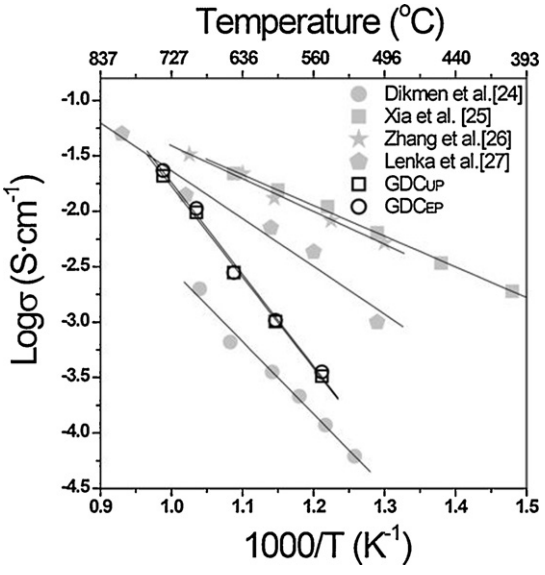

Fig. 9. Arrhenius plots of the total conductivities for the various $Gd_{0.1}Ce_{0.9}O_{2-\delta}$ samples in air.

The calculated values of the capacitance associated with the fitted semicircles for GDC_{UP} and GDC_{EP} are also summarized in Table 1. It was reported that the capacitance value of bulk, grain boundary, and electrode–electrolyte interface are of the order of 10^{-12}, 10^{-11} to 10^{-8}, and 10^{-7} to 10^{-4} F, respectively [23]. Considering the capacitance values of the fitted semicircles for GDC_{UP} and GDC_{EP}, it seems that (R_1CPE_1), (R_2CPE_2), and (R_3CPE_3) are related to the bulk, grain boundary, and the electrode–electrolyte interface.

As shown in Fig. 9, the electrical conductivity of the GDC_{EP} is similar to that of the GDC_{UP}. The electrical conductivity of the GDE_{UP} and GDC_{EP} are higher than that reported by Dikmen [24] but lower than those reported by others [25–27]. This result is believed to be related to the lower relative density (∼90%) compared to those (∼99%) of others [25–27].

4. Conclusion

Gadolinium doped ceria nanoparticles were successfully synthesized by aerosol flame deposition with electrostatic and ultrasonic atomization methods. Electrostatic atomization is shown to be the more effective atomization method in controlling the size of particles by changing electric field. Furthermore, the GDC pellet prepared with electrostatic atomization exhibited reduced grain size, crystallite size and similar electrical conductivity compared with ultrasonic atomization. These results suggest that electrostatic atomization in aerosol flame deposition offers a valuable route for the synthesis of smaller GDC particles for intermediate temperature solid oxide fuel cells.

Acknowledgements

It is supported by Solid oxide fuel cell of New & Renewable Energy R&D program (20093021030010) under the Korea Ministry of Knowledge Economy (MKE). Also, this work is the outcome of a Manpower Development Program for Energy supported by the Ministry of Knowledge and Economy (MKE).

References

[1] S.C. Singhal, Advances in solid oxide fuel cell technology, Solid State Ionics 135 (2000) 305–313.
[2] S. Zha, C. Xia, G. Meng, Effect of Gd (Sm) doping on properties of ceria electrolyte for solid oxide fuel cells, J. Power Sources 115 (2003) 44–48.
[3] I. Kosacki, T. Suzuki, H. Anderson, P. Colomban, Raman scattering and lattice defects in nanocrystalline CeO_2 thin films, Solid State Ionics 149 (2002) 99–105.
[4] T. Suzuki, I. Kosacki, H. Anderson, P. Colomban, Electrical conductivity and lattice defects in nanocrystalline cerium oxide thin films, J. Am. Ceram. Soc. 84 (2001) 2007–2014.
[5] H. Yoshida, T. Inagaki, K. Miura, M. Inaba, Z. Ogumi, Density functional theory calculation on the effect of local structure of doped ceria on ionic conductivity, Solid State Ionics 160 (2003) 109–116.
[6] J. Ma, T.S. Zhang, L.B. Kong, P. Hing, S.H. Chen, $Ce_{0.8}Gd_{0.2}O_{2-\delta}$ ceramics derived from commercial submicron-sized CeO_2 and Gd_2O_3 powders for use as electrolytes in solid oxide fuel cells, J. Power Sources 132 (2004) 71–76.
[7] Y.J. Kang, H.J. Park, G.M. Choi, The effect of grain size on the low-temperature electrical conductivity of doped CeO_2, Solid State Ionics 179 (2008) 1602–1605.
[8] Z. Tianshu, P. Hing, H. Huang, J. Kilner, Ionic conductivity in the CeO_2–Gd_2O_3 system ($0.05 \leq Gd/Ce \leq 0.4$) prepared by oxalate coprecipitation, Solid State Ionics 148 (2002) 567–573.
[9] K. Yamashita, K.V. Ramanujachary, M. Greenblatt, Hydrothermal synthesis and low temperature conduction properties of substituted ceria ceramics, Solid State Ionics 81 (1995) 53–60.
[10] D.H. Prasad, J.W. Son, B.K. Kim, H.W. Lee, J.H. Lee, Synthesis of nanocrystalline $Ce_{0.9}Gd_{0.1}O1.95$ electrolyte by novel sol–gel thermolysis process for IT-SOFCs, J. Eur. Ceram. Soc. 28 (2008) 3107–3112.
[11] R. Mueller, L. Madler, S.E. Pratsinis, Nanoparticle synthesis at high production rates by flame spray pyrolysis, Chem. Eng. Sci. 58 (2003) 1969–1976.
[12] L. Madler, H.K. Kammler, R. Muller, S.E. Pratsinis, Controlled synthesis of nanostructured particles by flame spray pyrolysis, J. Aerosol Sci. 33 (2002) 369–389.
[13] J. Cho, M.S. Choi, Determination of number density, size and morphology of aggregates in coflow diffusion flames using light scattering and local sampling, J. Aerosol Sci. 31 (2000) 1077–1095.
[14] H.D. Jang, H.C. Kim, Y.J. Suh, H.C. Kim, C.K. Lee, Synthesis of lithium–cobalt oxide nanoparticles by flame spray pyrolysis, Aerosol Sci. Technol. 38 (2004) 1027–1032.
[15] A.H. Lefebvre, Atomization and Spray, Taylor & Francis Press, New York, 1989.
[16] J.M. Im, Y.S. Yoon, D.W. Shin, Synthesis of nano-crystalline $Gd_{0.1}Ce_{0.9}O_{2-x}$ for IT-SOFC by aerosol flame deposition, Ceram. Int. 34 (2008) 877–881.
[17] Y. Liu, M. Liu, Porous electrodes for low-temperature solid oxide fuel cells fabricated by a combustion spray process, J. Am. Ceram. Soc. 87 (2004) 2139–2142.
[18] K. Wittmaack, Towards a realistic description of the contribution of primary and secondary aerosols to ambient particle number and mass distributions, J. Aerosol Sci. 35 (2004) 611–620.
[19] J.M. Im, H.J. You, Y.S. Yoon, D.W. Shin, Synthesis of nano-sized gadolinia doped ceria powder by aerosol flame deposition, J. Eur. Ceram. Soc. 27 (2007) 3671–3675.
[20] H.J. You, K.H. Cho, Y.S. Yoon, J.M. Im, D.W. Shin, Synthesis of yttria-stabilized zirconia film by aerosol flame pyrolysis deposition, J. Anal. Appl. Pyrolysis 81 (2008) 14–19.
[21] O.V. Salata, Tools of nanotechnology: electrospray, Curr. Nanosci. 1 (2005) 25–33.
[22] F. Yuan, L.C.H. Chen, Preparation of zirconia and yttria-stabilized zirconia (YSZ) fine powders by flame-assisted ultrasonic spray pyrolysis (FAUSP), Solid State Ionics 109 (1998) 119–123.
[23] R.S.J. Rang, J. Acoust. Soc. Am. 35 (1962) 6.
[24] D.R. Chen, D.Y.H. Pui, L. Kaufman, Electrospraying of conducting liquids for monodisperse aerosol generation in the 4 nm to 1.8 μm diameter range, J. Aerosol Sci. 26 (1995) 963–977.
[25] Q. Li, T. Xia, X.D. Liu, X.F. Ma, J. Meng, X.Q. Cao, Fast densification and electrical conductivity of yttria-stabilized zirconia nanoceramics, Mater. Sci. Eng. B 138 (2007) 78–83.
[26] S. Dikmen, P. Shuk, M. Greenblatt, H. Gocmez, Hydrothermal synthesis and properties of $Ce_{1-x}Gd_xO_{2-\delta}$ solid solutions, Solid State Sci. 4 (2002) 585–590.
[27] C. Xia, M. Liu, Microstructures, conductivities, and electrochemical properties of $Ce_{0.9}Gd_{0.1}O_2$ and GDC-Ni anodes for low-temperature SOFCs, Solid State Ionics 152–153 (2002) 423–430.